Quantitative Evaluation of Knee Subchondral Bone Mineral Density Using Cone Beam Computed Tomography

Mikael J. Turunen, Juha Töyräs, Harri T Kokkonen, and Jukka S. Jurvelin

***Abstract*— Contrast agent enhanced cone beam computed tomography (CE-CBCT), a technique capable of high-resolution *in vivo* imaging with small radiation dose, has been applied successfully for clinical diagnostics of cartilage degeneration, *i.e.*, osteoarthritis (OA). As an X-ray technique, CE-CBCT may also detect changes in mineral density of subchondral bone (volumetric bone mineral density, vBMD), known to be characteristic for OA. However, its feasibility for density measurements is not clear due to limited signal-to-noise ratio and contrast of CBCT images. In the present study, we created clinically applicable hydroxyapatite phantoms and determined vBMDs of cortical bone, trabecular bone, subchondral trabecular bone and subchondral plate of 10 cadaver (*ex vivo*) and 10 volunteer (*in vivo*) distal femora using a clinical CBCT scanner, and for reference, also using a conventional CT. Our results indicated strong linear correlations between the vBMD values measured with the CT and CBCT scanners ($R^2 > 0.90$, $p < 0.001$), however, absolute vBMD values were dependent on the scanner in use. Further, the differences between the vBMDs of cortical bone, trabecular bone and subchondral bone were similar and independent of the scanner. The present results indicate that the vBMD values might not be directly comparable between different instruments. However, based on our present and previous results, we propose that, for OA diagnostics, clinical CBCT enables not only quantitative analysis of articular cartilage but also subchondral bone vBMD. Quantitative information on both cartilage and subchondral bone could be beneficial in OA diagnostics.**

***Index Terms*— bone mineral density, computed tomography, cone beam computed tomography, femur, human, osteoarthritis, hydroxyapatite phantom**

I. Introduction

OSTEOARTHRITIS (OA) is a disease affecting all connective tissues in a joint. Changes of subchondral bone related to initiation and progress of OA are significant [1]–[3] and affect the integrity of the whole joint, including articular cartilage and menisci [4]. The density of subchondral bone may be elevated in OA due to sclerosis [5], cartilage defects [6] or during OA related thicknening of the cartilage [7]. Thus, quantitative information on the articular cartilage, menisci and underlying bone, e.g. bone mineral density (BMD), could be beneficial when diagnosing OA.

Contrast enhanced computed tomography (CECT) has been proposed for diagnostics of cartilage lesions and degeneration. Recently, contrast enhanced cone beam computed tomography (CE-CBCT) was applied successfully for clinical diagnostics of articular cartilage as well as for detection of osteochondral lesions [8]–[11]. As an X-ray technique, CE-CBCT may also provide a tool for early detection of OA related changes in subchondral bone. CBCT provides higher resolution with significantly lower costs than conventional CT or magnetic resonance imaging (MRI). For these reasons, it may have great potential in diagnostics of various pathological conditions of joints. Although CE-CBCT enables simultaneous imaging of all joint tissues, certain restrictions, such as limited signal-to-noise ratio and contrast resolution, of CE-CBCT [12] can jeopardize measurement of subchondral bone density during contrast enhanced imaging of cartilage [13], [14].

CECT has shown potential for quantitative diagnostics of early OA. It has been used to evaluate the composition of articular cartilage [15]–[18], to detect effects of mechanical injuries and degeneration [19], [20]. Furthermore, some in vitro attempts have been carried out for simultaneous evaluation of articular cartilage and subchondral bone [21].

Determination of BMD with a conventional computed tomography (CT) scanner requires use of calibration phantoms. Unfortunately, most clinical phantoms are designed for full body CTs, making them too large for quantitative imaging of joints with clinical CBCT scanners. Further, densities of these phantoms may not cover a range wide enough for analysis of high density bone. Some common clinical phantoms can mimic the apparent density, but the substance does not match with the calcium hydroxyapatite (HA) in bone. This results in errors in determined BMD values.

In the present study, our aim was to clarify the feasibility of CBCT for measurement of volumetric BMD (vBMD) in subchondral, trabecular and cortical bone. Especially, we hypothesized that CBCT enables quantitative determination of subchondral bone density with good enough accuracy to detect

This work was supported by Academy of Finland (project 269315).

M. J. Turunen (e-mail: mikael.turunen@uef.fi) is with the Department of Applied Physics, University of Eastern Finland, FI-70211, Kuopio, Finland.

J. Töyräs and J. S. Jurvelin are with the Department of Applied Physics, University of Eastern Finland, FI-70211, Kuopio, Finland and also with the Diagnostic Imaging Centre, Kuopio University Hospital, FI-70029, Kuopio, Finland.

H.T. Kokkonen is with the Diagnostic Imaging Centre, Kuopio University Hospital, FI-70029, Kuopio Finland.

changes related to OA.

II. Materials and Methods

The study design was divided into three parts: 1) creation of HA phantoms, 2) determination of the vBMDs of the phantoms using dual energy x-ray absorptiometry (DXA), and 3) determination of vBMDs of different regions in distal femur ex vivo and in vivo using conventional clinical CT and CBCT scanners (Fig. 1).

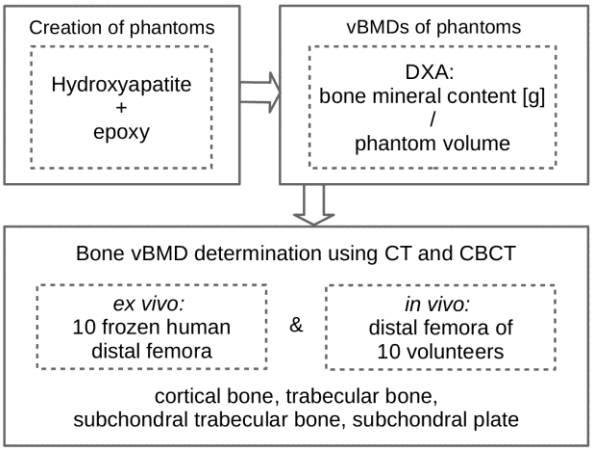

Fig. 1. Flowchart of the study design.

A. Creation of Phantoms

Five phantoms with different vBMDs were created by weighing 500, 1000, 1500 and 2000 mg of synthetic hydroxyapatite powder (reagent grade, Sigma-Aldrich Inc., St Louis, MO) and mixing it with epoxy in 2 ml Eppendorf tubes, resulting in 2 ml of HA powder-epoxy mix in each tube. After the mixing, the tubes were set into a programmable rotator-mixer (Grant Bio PTR-30, Keison Products, Chelmsford, UK) to prevent gravitation driven deposition of the HA powder and were let to congeal for 72 hours in room temperature. Subsequently, the tubes were exposed to 100 for 12 hours to finalize the solidification. The tubes were cut open and the ends of the phantoms were flattened with a saw. The diameters and volumes of these cylindrical shaped phantoms were 8.90 ± 0.03 mm and 1.73 ± 0.04 cm^3 (mean ± SD), respectively.

B. Determination of Phantoms vBMD

The bone mineral contents (BMC [g]) of the HA phantoms were determined using DXA (GE Healthcare Lunar iDXA, Madison, WI). The BMCs were normalized with the volume (DXA image slice area multiplied with phantom height) to determine reference vBMD [g/cm^3] of each phantom. Earlier, we have found DXA to provide accurate information on mineral density of small bone samples [22].

C. Determination of Bone vBMD

For the vBMD determination *ex vivo*, ten frozen human distal femora (age 29-74 years, 9 men and 1 woman) were imaged using 1) a conventional CT (Siemens Somatom Definition Edge, Siemens, Germany) scanner and 2) a clinical CBCT (Verity, Planmed Oy, Helsinki, Finland) scanner both together with the HA phantoms. The CT measurements were conducted using tube voltage of 120 kV and 80 mAs with a voxel size of ~326 µm x 326 µm x 500 µm (depending of the size of the scan area). Correspondingly, the CBCT measurements were conducted using tube voltage of 96 kV and 72.5 mAs with a voxel size of 200 µm x 200 µm x 200 µm. A routine clinical scanning protocol was used with both scanners. A custom made band with small individual pockets for the HA phantoms, arranged in order from less dense to highest density separated by 2 cm from each other, was designed for clinical use and wrapped around the distal femur. After imaging, four volumes of interest (VOIs) were segmented from the image-stacks using Mimics (v12.3, Materialise, Leuven, Belgium): cortical bone (shaft), trabecular bone (medial condyle, cylindrical area), subchondral plate and subchondral trabecular bone (lateral condyle) (Fig. 2). The VOIs in each knee were controlled visually by comparison of the created masks in CT and CBCT image-stacks and they were modified until a visual match was obtained. From each image-stack, the average Hounsfield units of the phantoms and the segmented bone VOIs were calculated. In HU analyses of phantoms, the diameter of the analyzed region (excluding the edges to avoid the beam hardening effect and partial volume averaging) was 16 and 9-16 voxels in CBCT and CT, respectively. vBMD analysis, using CT and CBCT image-stacks, confirmed the homogeneous HA distribution in the phantoms. Moreover, the full phantom length HU values were derived to minimize the possible effect of any inhomogeneity. The vBMDs of different VOIs were determined using the image-stack specific calibration curves based on the HA phantoms. vBMD of all pixels in each measured knee (Fig. 3A-B), using the respective calibration curves (Fig. 3C-D), could thus be determined. All data (calibration and vBMD determination) was analyzed with MATLAB (R2012b,

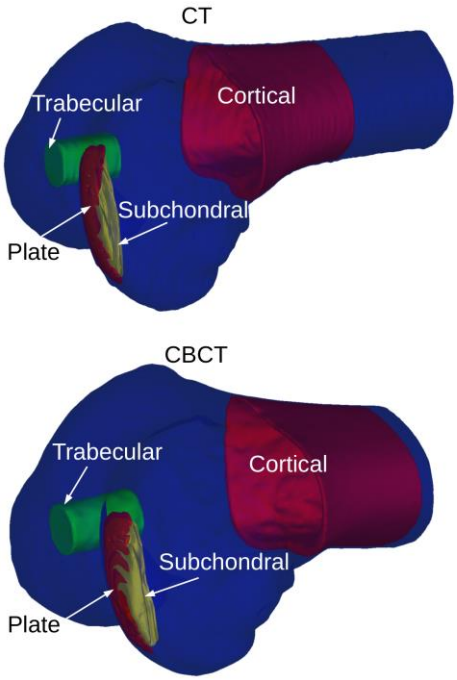

Fig. 2. Three-dimensional masks for vBMD analysis of cortical bone (Cortical), trabecular bone (Trabecular), subchondral trabecular bone (Subchondral) and subchondral plate (Plate) in a knee imaged with CT and CBCT scanners.

MathWorks, Inc., MA).

For the vBMD determination *in vivo*, ten volunteer subjects (age 22-75 years, 5 men and 5 women) with no indications of osteoporosis or osteoarthritis were recruited. The ethical committee of Kuopio University Hospital had a favorable opinion on the study protocol (decision number: 54/2011). The distal femora from the right leg were imaged using CT (tube voltage of 120 kV, and voxel size of ~515 µm x 515 µm x 500 µm (depending on the size of the scan area)). Tube current modulation (CARE Dose4D) was used. Subsequently, the knees were imaged with CBCT (tube voltage of 96 kV, 45.3 mAs and voxel size of 400 µm x 400 µm x 400 µm). For comparison, the average effective radiation doses for CT and CBCT imaging were estimated to be 0.04 mSv and 0.02 mSv, respectively. The positioning of the HA phantoms was similar as for *ex vivo* measurements (Fig. 3). Procedures for segmentation and vBMD calculations were similar as those used for *ex vivo* data.

The sizes of the VOIs in *ex vivo* measurements were 11.0 ± 2.0, 1.4 ± 0.2, 1.1 ± 0.4 and 0.18 ± 0.08 cm^3 (mean ± SD) for cortical bone, trabecular bone, subchondral bone and subchondral plate, respectively. The corresponding values in *in vivo* measurements were 9.2 ± 1.3, 1.9 ± 0.4, 1.9 ± 0.5 and 0.36 ± 0.14 cm^3. Thus, the voxel count in the VOIs varied from 2442 (subchondral plate) to 253170 (cortical bone). To avoid partial

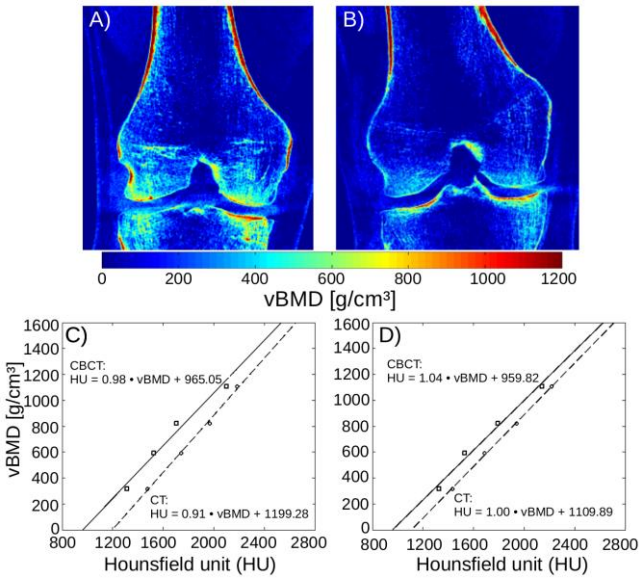

Fig. 3. CBCT analysis. Two-dimensional *in vivo* vBMD images of knees with normal (30 years old man, average vBMD in the study population) A) and low (44 years old pre-menopausal woman, lowest vBMD in the study population) B) vBMDs and respective calibration curves C) and D) (solid lines and with squares). Additionally, CT calibration curves are also shown (dashed lines with circles). Regression equations of all calibration curves are presented.

volume averaging, cortical bone and subchondral plate were segmented from the bone marrow and surrounding tissues, excluding the voxels at the edge of bone tissue. Trabecular bone and subchondral bone were segmented as full tissue due to resolution restrictions for trabecular bone tissue vBMD [23].

D. Statistical Analysis

Linear correlations (Pearson) between the bone vBMD values, as determined using the CT and CBCT scanners, were calculated. Wilcoxon signed ranks test was used to compare the phantom and bone vBMD values, as measured with the two scanners. Additionally, Bland-Altman plots were created and analyzed for agreement between the vBMD values determined using CT and CBCT scanners. In all statistical analyses $p < 0.05$ was considered as the limit for statistical significance. All statistical analyses were performed using SPSS (IBM SPSS, v. 21, Armonk, NY).

III. Results

In distal femora *ex vivo* measurements, the vBMD values were significantly higher in subchondral bone and subchondral plate when determined with CBCT compared to CT (Fig. 4A). For *in vivo* measurements, the vBMD values determined with CBCT were significantly lower in subchondral plate and cortical bone when compared to CT vBMD values (Fig. 4B).

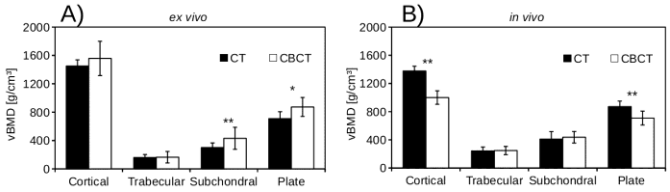

Fig. 4. vBMDs of *ex vivo* A) and *in vivo* B) measurements using CT and CBCT at different regions of interests using HA phantoms. Wilcoxon signed ranks test ** $p < 0.01$, * $p < 0.05$.

The linear correlation between vBMDs determined with CT and CBCT *ex vivo* was significant (R^2 = 0.90, $p < 0.001$). Similarly, the correlation in *in vivo* data was also significant (R^2 = 0.92, $p < 0.001$). The average vBMDs determined using CBCT were somewhat higher in *ex vivo* and lower in *in vivo*, compared to values determined using CT (Fig. 5).

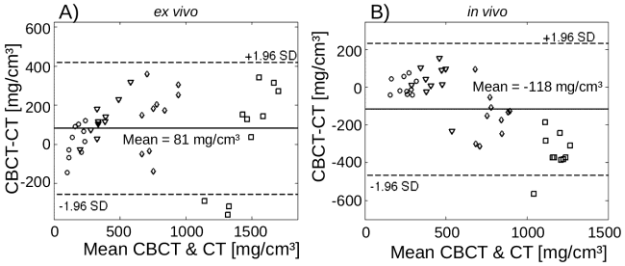

Fig. 5. Bland-Altman plots showing the mean vs differences of vBMDs determined with CT and CBCT *ex vivo* A) and *in vivo* B). The mean difference with ± 1.96 SD is shown. In the *in vivo* measurements, a slight underestimation for high vBMDs is found. In the *ex vivo* measurements, no clear trend is observed. vBMDs from different VOIs are shown with different markers: cortical bone (square), trabecular bone (circle), trabecular subchondral bone (triangle) and subchondral plate (diamond).

IV. Discussion

Significant differences between the bone vBMDs determined with CT and CBCT were evident in each VOI in ex vivo measurements (Fig. 4(A)). However, the differences in vBMD values between VOIs were similar irrespective of the scanner in use. This implicates that the vBMD values measured with CBCT could be used to detect anomalies in spatial variation of

vBMD, e.g. sclerosis of subchondral bone, which could be used in diagnosis of OA.

The vBMDs determined in vivo agreed with those measured ex vivo with one major difference; vBMD of cortical bone was significantly underestimated in CBCT measurement in vivo This is most likely due to beam hardening and scattering, more prominent in CBCT than in CT. Based on the comparison with CT, CBCT can determine the vBMD in trabecular and subchondral bone. With higher densities, i.e. cortical bone and subchondral plate, the in vivo vBMDs are underestimated with CBCT. However, CBCT can distinguish these areas from each other based on vBMD. In ex vivo samples, vBMDs determined with CBCT is more comparable with CT, even small overestimation in subchondral trabecular bone and subchondral plate is evident. The dynamic range of vBMD measurements by CBCT is more limited than that of the conventional CT. This is shown by an obvious trend, especially in in vivo measurements, in the Bland-Altman plots (Fig. 5). However, the vBMD values by CBCT could distinguish the different VOIs in two knees measured in vivo (Fig. 3(A)–(B)). Furthermore, lower radiation dose, reduced costs, potential for higher resolution and portability are benefits of CBCT when compared to conventional CT. Despite the strong correlations and comparable averages in vBMD between CT and CBCT (Fig. 4), the Bland-Altman plots (Fig. 5) present a relatively high variation between the individual VOIs. These results encourage to further improve the accuracy of CBCT in determination of bone density.

Compared to conventional CT, the resolution is higher, radiation doses and imaging times are lower and costs are significantly reduced in CBCT. Furthermore, CBCT joint imaging is a relatively new technique and efforts are constantly made to increase image resolution together with the improved signal-to-noise ratio, e.g. by adding collimators, control for radiation dose, filtering, optimum imaging parameters and phantom combinations, and developing algorithms for correction of beam hardening [24], [25]. Thus, potential of CBCT for clinical diagnosis of joint conditions may still be improved in the future.

Known amounts of HA powder were weighed and mixed with epoxy to create five phantoms with different densities. Due to some uncontrolled stages in the phantom creation process, e.g. possible vaporization of the epoxy during the solidification, the phantoms were subsequently imaged with DXA to determine their true vBMDs. In our previous study, it was found that DXA measures mineral density of small bone samples accurately [22]. In the present study, vBMD values of the phantoms determined with DXA were used for calibration in the CT and CBCT measurements.

Subchondral bone density may be elevated in OA subjects, compared to healthy subjects, especially when sclerosis is present [5], and with prevalent cartilage defects [6]. Recently, it has been reported that high subchondral bone density is associated with increased cartilage thickness in subjects with radiographic OA [7]. In osteoporosis the radiographic BMD decreases. Osteoporosis affects first bone with high turnover rate [26], thus vBMD changes are first expected in trabecular and subchondral trabecular bone areas. With progressing osteoporosis also the BMD of higher density areas, i.e. bone cortices, is diminished.

Our present results indicate that the vBMD values might not be comparable between CT and CBCT scanners. However, CBCT imaging, coupled with HA phantoms, shows potential in detection of quantitative changes in vBMD, and potentially also OA related changes in subchondral bone. The present CBCT technique could indicate the differences in vBMD of cortical, trabecular and subchondral bone. Especially in diagnostics of OA and knee injuries, quantitative and qualitative information on subchondral bone, together with diagnostics of articular cartilage and meniscus [8]–[11], [18], could improve understanding on role of different joint structures in cartilage degeneration.

REFERENCES

[1] M. Mahjoub, F. Berenbaum, and X. Houard, "Why subchondral bone in osteoarthritis? The importance of the cartilage bone interface in osteoarthritis," Osteoporos. Int., vol. 23 Suppl 8, pp. S841–6, Dec. 2012.

[2] Y. Henrotin, L. Pesesse, and C. Sanchez, "Subchondral bone and osteoarthritis: biological and cellular aspects," Osteoporos. Int., vol. 23 Suppl 8, pp. S847–51, Dec. 2012.

[3] V. Bousson, T. Lowitz, L. Laouisset, K. Engelke, and J.-D. Laredo, "CT imaging for the investigation of subchondral bone in knee osteoarthritis," Osteoporos. Int., vol. 23 Suppl 8, pp. S861–5, Dec. 2012.

[4] M. S. Venäläinen, M. E. Mononen, J. S. Jurvelin, J. Töyräs, T. Virén, and R. K. Korhonen, "Importance of material properties and porosity of bone on mechanical response of articular cartilage in human knee joint--a two-dimensional finite element study," J. Biomech. Eng., vol. 136, no. 12, p. 121005, Dec. 2014.

[5] S. Clarke, C. Wakeley, J. Duddy, M. Sharif, I. Watt, K. Ellingham, C. J. Elson, G. Nickols, and J. R. Kirwan, "Dual-energy X-ray absorptiometry applied to the assessment of tibial subchondral bone mineral density in osteoarthritis of the knee," Skeletal Radiol., vol. 33, no. 10, pp. 588–95, Oct. 2004.

[6] D. Dore, S. Quinn, C. Ding, T. Winzenberg, and G. Jones, "Correlates of subchondral BMD: a cross-sectional study," J. Bone Miner. Res., vol. 24, no. 12, pp. 2007–15, Dec. 2009.

[7] Y. Cao, O. P. Stannus, D. Aitken, F. Cicuttini, B. Antony, G. Jones, and C. Ding, "Cross-sectional and longitudinal associations between systemic, subchondral bone mineral density and knee cartilage thickness in older adults with or without radiographic osteoarthritis," Ann. Rheum. Dis., vol. 73, no. 11, pp. 2003–9, Nov. 2014.

[8] H. T. Kokkonen, a. S. Aula, H. Kroger, J.-S. Suomalainen, E. Lammentausta, E. Mervaala, J. S. Jurvelin, and J. Toyras, "Delayed Computed Tomography Arthrography of Human Knee Cartilage *In vivo*," Cartilage, vol. 3, no. 4, pp. 334–341, May 2012.

[9] H. Kokkonen, J. Suomalainen, A. Joukainen, H. Kröger, J. Sirola, J. Jurvelin, J. Salo, and J. Töyräs, "*In vivo* diagnostics of human knee cartilage lesions using delayed CBCT arthrography," J. Orthop. Res., vol. 32, no. 3, pp. 403–12, Mar. 2014.

[10] A. S. Kallioniemi, J. S. Jurvelin, M. T. Nieminen, M. J. Lammi, and J. Töyräs, "Contrast agent enhanced pQCT of articular cartilage," Phys. Med. Biol., vol. 52, no. 4, pp. 1209–19, Feb. 2007.

[11] E. K. J. Tuominen, J. Kankare, S. K. Koskinen, and K. T. Mattila, "Weight-bearing CT imaging of the lower extremity," AJR. Am. J. Roentgenol., vol. 200, no. 1, pp. 146–8, Jan. 2013.

[12] W. De Vos, J. Casselman, and G. R. J. Swennen, "Cone-beam computerized tomography (CBCT) imaging of the oral and maxillofacial region: A systematic review of the literature," Int. J. Oral Maxillofac. Surg., vol. 38, no. 6, pp. 609–625, Jun. 2009.

[13] J. T. Hsu, S. P. Wang, H. L. Huang, Y. J. Chen, J. Wu, and M. T. Tsai, "The assessment of trabecular bone parameters and cortical bone strength: A comparison of micro-CT and dental cone-beam CT," J. Biomech., vol. 46, no. 15, pp. 2611–2618, Oct. 2013.

[14] Y. Hua, O. Nackaerts, J. Duyck, F. Maes, and R. Jacobs, "Bone quality assessment based on cone beam computed tomography imaging," Clin. Oral Implant. Res, vol. 20, no. 8, pp. 767–771, Aug. 2009.

[15] T. S. Silvast, J. S. Jurvelin, a S. Aula, M. J. Lammi, and J. Töyräs, “Contrast agent-enhanced computed tomography of articular cartilage: association with tissue composition and properties,” Acta radiol., vol. 50, no. 1, pp. 78–85, Jan. 2009.

[16] P. N. Bansal, N. S. Joshi, V. Entezari, M. W. Grinstaff, and B. D. Snyder, “Contrast enhanced computed tomography can predict the glycosaminoglycan content and biomechanical properties of articular cartilage,” Osteoarthritis Cartilage, vol. 18, no. 2, pp. 184–91, Feb. 2010.

[17] P. N. Bansal, N. S. Joshi, V. Entezari, B. C. Malone, R. C. Stewart, B. D. Snyder, and M. W. Grinstaff, “Cationic contrast agents improve quantification of glycosaminoglycan (GAG) content by contrast enhanced CT imaging of cartilage,” J. Orthop. Res., vol. 29, no. 5, pp. 704–9, May 2011.

[18] B. A. Lakin, D. J. Grasso, R. C. Stewart, J. D. Freedman, B. D. Snyder, and M. W. Grinstaff, “Contrast enhanced CT attenuation correlates with the GAG content of bovine meniscus,” J. Orthop. Res., vol. 31, no. 11, pp. 1765–71, Nov. 2013.

[19] H. T. Kokkonen, J. Mäkelä, K. A. M. Kulmala, L. Rieppo, J. S. Jurvelin, V. Tiitu, H. M. Karjalainen, R. K. Korhonen, V. Kovanen, and J. Töyräs, “Computed tomography detects changes in contrast agent diffusion after collagen cross-linking typical to natural aging of articular cartilage,” Osteoarthritis Cartilage, vol. 19, no. 10, pp. 1190–8, Oct. 2011.

[20] H. T. Kokkonen, J. S. Jurvelin, V. Tiitu, and J. Töyräs, “Detection of mechanical injury of articular cartilage using contrast enhanced computed tomography,” Osteoarthritis Cartilage, vol. 19, no. 3, pp. 295–301, Mar. 2011.

[21] A. S. Aula, J. S. Jurvelin, and J. Töyräs, “Simultaneous computed tomography of articular cartilage and subchondral bone,” Osteoarthritis Cartilage, vol. 17, no. 12, pp. 1583–8, Dec. 2009.

[22] J. Töyräs, H. Kröger, and J. S. Jurvelin, “Bone properties as estimated by mineral density, ultrasound attenuation, and velocity,” Bone, vol. 25, no. 6, pp. 725–31, Dec. 1999.

[23] H. Isaksson, J. Töyräs, M. Hakulinen, A.S. Aula, I. Tamminen, P. Julkunen, H. Kröger, and J. S. Jurvelin, ”Structural parameters of normal and osteoporotic human trabecular bone are affected differently by microCT image resolution,” Osteoporos. Int., vol. 22, no. 1, pp. 167-177, Jan. 2011.

[24] U.S. Department of Health and Human Services, “Bone Health and Osteoporosis: A report of the Surgeon General,” Rockville, MD: U.S. Department of Health and Human Services, Office of the Surgeon General, 2004.

[25] J. Hsieh, R. C. Molthen, C. A. Dawson, and R. H. Johnson, “An iterative approach to the beam hardening correction in cone beam CT,” Med. Phys., vol. 27, no. 1, pp. 23–9, Jan. 2000.

[26] J. S. Maltz, B. Gangadharan, S. Bose, D. H. Hristov, B. A. Faddegon, A. Paidi, and A. R. Bani-Hashemi, “Algorithm for X-ray scatter, beam-hardening, and beam profile correction in diagnostic (kilovoltage) and treatment (megavoltage) cone beam CT,” IEEE Trans. Med. Imaging, vol. 27, no. 12, pp. 1791–810, Dec. 2008.